Decay of spin coherences in one-dimensional spin systems

2013 New J. Phys. 15 093035

(http://iopscience.iop.org/1367-2630/15/9/093035)

New Journal of Physics
The open access journal for physics

Decay of spin coherences in one-dimensional spin systems

G Kaur, A Ajoy and P Cappellaro[1]
Department of Nuclear Science and Engineering, Massachusetts Institute of Technology, Cambridge, MA 02139, USA
E-mail: pcappell@mit.edu

New Journal of Physics **15** (2013) 093035 (14pp)
Received 9 June 2013
Published 23 September 2013
Online at http://www.njp.org/
doi:10.1088/1367-2630/15/9/093035

Abstract. Strategies to protect multi-qubit states against decoherence are difficult to formulate because of their complex many-body dynamics. A better knowledge of the decay dynamics would help in the construction of dynamical decoupling control schemes. Here we use solid-state nuclear magnetic resonance techniques to experimentally investigate decay of coherent multi-spin states in linear spin chains. Leveraging on the quasi-one-dimension geometry of fluorapatite crystal spin systems, we can gain a deeper insight on the multi-spin states created by the coherent evolution, and their subsequent decay, than it is possible in three-dimensional (3D) systems. We are then able to formulate an analytical model that captures the key features of the decay. We can thus compare the decoherence behavior for different initial states of the spin chain and link their decay rate to the state characteristics, in particular their coherence and long-range correlation among spins. Our experimental and theoretical study shows that the spin chains undergo a rich dynamics, with a slower decay rate than for the 3D case, and thus might be more amenable to decoupling techniques.

[1] Author to whom any correspondence should be addressed.

Contents

1. Introduction

Large quantum systems hold the promise to deliver improvements in computation and in metrology, by exploiting entangled or squeezed states. Unfortunately these quantum systems are usually very fragile and plagued by problems of decoherence [1]—as they undergo irreversible decay [2] due to interaction with their environment. The decay of single qubits under the effect of various types of environments have been extensively studied and control sequences that could mitigate decoherence effects have been introduced (e.g. dynamical decoupling techniques [3–6]). However, large scale quantum information processing systems will require the preparation and control of *multi-qubit* states. These states are harder to control and to model analytically because of their complex many-body dynamics. While some recent works have looked at their decoherence and control schemes via dynamical decoupling [7], the decay was usually assumed to be induced by an uncorrelated bath, acting independently on each qubit, although this is often not the case in nature, especially for spatially close spins. In this paper, we experimentally and theoretically study the decay of such multi-qubit states under the action of a correlated spin bath. In particular, we are interested in investigating the decay rate dependence on the correlations in a multi-qubit spin state. We leverage the low dimensionality of the system studied—the linear coupling geometry provided by nuclear spins in apatite crystals [8, 9]—to gain insight into both the many-body states created by the coherent Hamiltonian dynamics and their ensuing decay. We present a simple analytical model that captures the essential features of the multi-qubit decays and compares well with the experimental data. These results will be helpful in paving the way for the future design of schemes to mitigate the decay.

Specifically, in a linear spin system—calcium fluorapatite (FAp) [10]—we consider multi-spin states created by the double quantum (DQ) Hamiltonian $\mathcal{H}_{\mathrm{DQ}}$, which has been widely studied in quantum transport [11]. We analyze their decay under the natural dipolar Hamiltonian $\mathcal{H}_{\mathrm{dip}}$. Similar decay dynamics were studied in more complex three-dimensional (3D) spin systems [12–15] and extended to the study of localization phenomena [16, 17]. However, in

contrast to 3D systems, the highly restricted coupling topology in our experiments leads to analytically tractable solutions for the Hamiltonian evolution and the decay rates. It is thus possible to have a much better characterization of the multi-spin states we can create than it was possible in more complex 3D systems. As a result we can study how the decay rate changes with the state characteristics, such as long-range correlations in extended spin clusters and their degree of coherence. This is also important in light of recent work in creating low-dimensional systems in ion-traps [18], or via Hamiltonian engineering [19] in crystals.

The paper is organized as follows. We describe the experimental system and methods and present the experimental results in section 2. In section 3 we introduce an analytical model (extended details can be found in the appendix) to interpret the experimental results. This leads us to a better insight into the decay rate dependence on the state characteristics that we further explore in section 4 by experimentally studying a diverse set of states.

2. Experimental methods and results

2.1. The spin system

The system of interest are ^{19}F nuclear spins in a single crystal of FAp [$Ca_5(PO_4)_3F$]. We use nuclear magnetic resonance (NMR) techniques to study the spin dynamics at room temperature in a 300 MHz Bruker Avance spectrometer ($B_0 = 7$T) with a probe tuned to 282.4 MHz. In the FAp crystal, six parallel chains lie along the crystal c-axis, with a short intra-nuclear spacing within a single chain, $r_0 = 0.3442$ nm, and a longer inter-chain separation of $R = 0.9367$ nm. The spins interact via the secular dipole–dipole Hamiltonian

$$\mathcal{H}_{\rm dip} = \sum_{ij} b_{ij}[2\sigma_z^i\sigma_z^j - (\sigma_x^i\sigma_x^j + \sigma_y^i\sigma_y^j)], \tag{1}$$

where σ_α^i are the usual Pauli matrices and the couplings are

$$b_{ij} = \frac{\mu_0}{16\pi}\frac{\gamma^2\hbar}{r_{ij}^3}(1 - 3\cos^2\vartheta_{ij}),$$

with μ_0 the standard magnetic constant, γ the ^{19}F gyromagnetic ratio, r_{ij} the distance between nucleus i and j and ϑ_{ij} the angle between $\vec{r}_{ij}$ and the z-axis. When the crystal is aligned with the magnetic field, as in our experiments, the nearest-neighbor (NN) inter-chain dipolar coupling is about 40 times weaker than the in-chain coupling. Thus, for short evolution times, couplings across different chains can be neglected and the system can be considered as a collection of one-dimensional (1D) spin chains [9, 20–23].

2.2. Experimental protocol

The experimental scheme is shown in figure 1. The system is first prepared in a suitable initial state $\rho_{\rm i}$ starting from its equilibrium thermal state. Evolution under a propagator $U_{\rm MQ}$ for a time τ creates a complex, multiple-quantum coherence state [24]. The system is then let to evolve freely for a time t, during which the coherences decay mainly under the effects of the dipolar Hamiltonian. In order to observe this decay, we first refocus the remaining coherences with a propagator $U_{\rm MQ}^\dagger$ before measuring the spin magnetization via the usual free-induction decay.

The equilibrium state is the Zeeman thermal state, $\rho_{\rm th}(0) \propto \exp(-\varepsilon\Sigma_z) \approx \mathbb{1} - \varepsilon\Sigma_z$, where $\Sigma_z = \sum_j \sigma_z^j$ and $\varepsilon = \gamma B_0/k_{\rm B}T \ll 1$ (with $k_{\rm B}$ the Boltzmann constant and T the temperature).

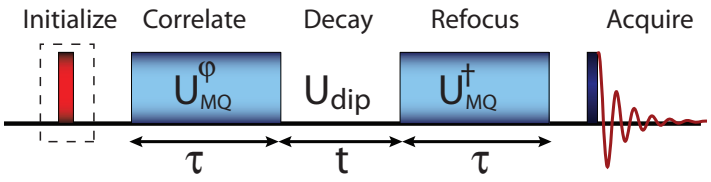

Figure 1. Experimental scheme. The system is first prepared in an initial state of interest, for example the thermal equilibrium state or $\sum \sigma_x$ using a $\pi/2$-pulse (red bar). Evolution via the DQ Hamiltonian $\mathcal{H}_{\rm DQ}$ (obtained by a multi-pulse sequence, blue rectangles) creates spin correlations during the time τ. A phase shift φ of the propagator encodes information about the multiple quantum coherence intensities created. The state undergoes decay under the dipolar interaction $\mathcal{H}_{\rm dip}$ during the time t. The correlated state is refocused by the inverse propagator $U^{\dagger}_{\rm DQ}$ before a $\pi/2$ pulse is used to detect the spin free-induction decay.

We focus on the evolution and decay of the deviation from identity of this state, i.e. $\delta\rho_{\rm th} \sim \Sigma_z$, and of other initial states that can be created from $\delta\rho_{\rm th}$ with appropriate manipulation (see section 4). Indeed, the identity does not evolve and does not contribute to the signal.

Starting from the prepared initial state $\rho_{\rm i}$, we create spin correlations by evolution under the DQ Hamiltonian

$$\mathcal{H}_{\rm DQ} = \sum_{ij} b_{ij}(\sigma^i_x\sigma^j_x - \sigma^i_y\sigma^j_y) \tag{2}$$

which is known to generate quantum coherences among the spins [24]. The primitive pulse cycle is given by, $P_2 = \frac{\delta t}{2} - \frac{\pi}{2}|_x - \delta t' - \frac{\pi}{2}|_x - \frac{\delta t}{2}$, where $\delta t' = 2\delta t + w$, δt is the delay between pulses and w is the width the $\pi/2$ pulse. We used the symmetrized eight-pulse variant of this basic sequence [24, 25], $P_8 = P_2 \cdot \overline{P_2} \cdot \overline{P_2} \cdot P_2$ (where $\overline{P_2}$ is the time-reversed version of P_2), which simulates $\mathcal{H}_{\rm DQ}$ to second order in the Magnus expansion [26]. In the experiments, the length of the $\pi/2$ pulse was $w = 1.01\,\mu$s and the evolution time was incremented by varying the inter-pulse delay from $\delta t = 1$ to $6.2\,\mu$s and the number of cydes was increased from 1 to 12 (varying both parameters enabled exploring a wide range of evolution times up to 1 ms). A recycle delay of 5 s was used to re-equilibrate the system.

The density operator created by evolution under the DQ Hamiltonian can be decomposed into its multiple quantum coherences (MQC) components, $\rho(\tau) = U_{\rm MQ}(\tau)\rho(0)U^{\dagger}_{\rm MQ}(\tau) = \sum_m \rho^{(m)}$, where a multiple quantum term of order m, $\rho^{(m)}$, acquires a phase $m\varphi$ under a collective Σ_z rotation by an angle φ. The correlated spin states created under $\mathcal{H}_{\rm DQ}$ evolution contain in general all *even* M coherence orders. However, since standard NMR techniques measure only single-quantum coherences (SQC), in order to probe the higher spin coherences it is necessary to indirectly encode their signatures into SQCs which can be measured inductively [27]. This is achieved by labeling each coherence order with a different phase φ by means of collective rotations $U_\varphi = \exp(-{\rm i}\varphi\Sigma_z/2)$ about the z-axis, effectively creating the phase shifted DQ Hamiltonian, $\mathcal{H}^{\varphi}_{\rm DQ} = U_\varphi\mathcal{H}_{\rm DQ}U^{\dagger}_\varphi$. Finally, MQC are refocused back to single-spin single-quantum terms and the free induction decay is measured. Each measurement is repeated while incrementing φ from 0 to 2π in steps of $\delta\varphi = 2\pi/2K$ where K is the highest

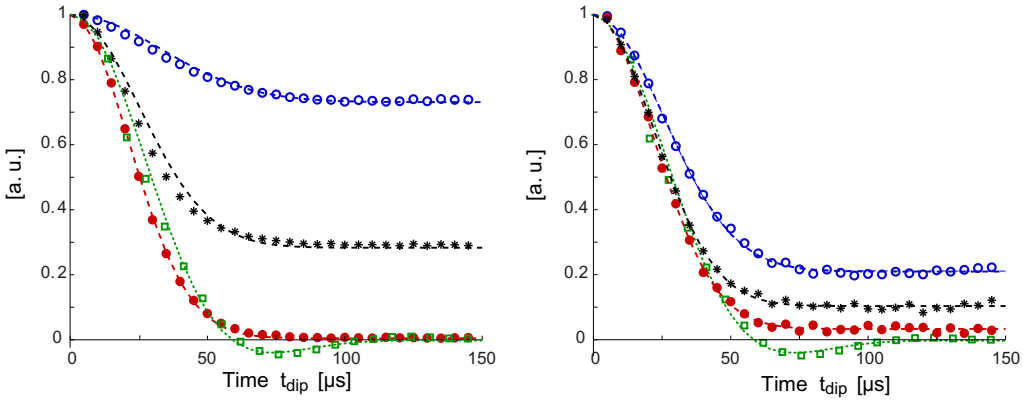

Figure 2. Normalized decay of quantum coherences created from the thermal initial state by evolving for a time τ under the $\mathcal{H}_{DQ}$ Hamiltonian. (ZQ blue open circles, DQ red dots, total signal black stars). Data points are the normalized signal intensities for evolution time $\tau = 48\,\mu$s (left) and $\tau = 589\,\mu$s (right). The dashed lines are fitting using the function in equation (5). For comparison we plot the free induction decay (green squares) that we fit with the function [28] $A[(1-C)\mathrm{sinc}(m_2 t)\,\mathrm{e}^{-m_1 t^2/2} + C]$, which corresponds to a second moment given by $M = m_1 + m + 2^{2/3}$.

order of MQC we wish to encode. If $\delta\rho_i$ is the initial density matrix, the final density matrix $\delta\rho_f$ is given by

$$\delta\rho_f(t,\tau) = U^{\dagger}_{MQ}(\tau)U_{dip}(t)U^{\varphi}_{MQ}(\tau)\delta\rho_i U^{\varphi\dagger}_{MQ}(\tau)U^{\dagger}_{dip}(t)U_{MQ}(\tau), \tag{3}$$

where $U_{MQ}(\tau) = \exp(-i\mathcal{H}_{DQ}\tau)$.

Since often the observable $\delta\rho_o$ is proportional to the initial state (as it is the case for the thermal equilibrium state and the total magnetization along the z-axis) we can write the measured signal as a correlation $S(t,\tau) = \mathrm{Tr}\{\delta\rho_f(t,\tau)\delta\rho_o(\tau)\}$, between the state prepared by the DQ evolution, $\delta\rho_o(\tau) = U_{MQ}(\tau)\delta\rho_o U^{\dagger}_{MQ}(\tau)$ and the same state after decay under the dipolar evolution, $\delta\rho_f(t,\tau) = U_{dip}\delta\rho_i(\tau)U^{\dagger}_{dip}$. The signal intensities of various coherence orders are thus given by the Fourier transform with respect to the phase φ:

$$I^{(m)}(t,\tau) = \mathrm{Tr}\{\delta\rho_o^{(m)}(\tau)\delta\rho^{(m)}(t,\tau)\} = \sum_{k=1}^{K} S^k(t,\tau)\mathrm{e}^{-\mathrm{i}km\delta\varphi}, \tag{4}$$

where $S^k(t,\tau) = \mathrm{Tr}\{\delta\rho_f^k(t,\tau)\delta\rho_o\}$ is the signal acquired in the kth measurement when setting $\varphi = \pi k/K$.

2.3. Results and data analysis

We first studied the decay of MQC intensities created under $\mathcal{H}_{DQ}$ starting from an initial thermal state ($\delta\rho_{th} \sim \Sigma_z$). In a quasi-1D system such as FAp, it is known that the DQ Hamiltonian excites mainly zero-quantum (ZQ) and DQ coherences [20, 29]. The decay of the total signal, $S(t,\tau) = \mathrm{Tr}\{\rho_f(t,\tau)\rho_o\}$, and of each coherence intensity is shown in figure 2 as a function of dipolar decay time (t) for two exemplary MQC excitation times, $\tau = 48$ and $589\,\mu$s.

The decoherence dynamics was studied by repeating the experimental scheme described above, while varying the DQ evolution time (τ) from 36 to 925 μs and the decay time (t) from 0 to 145 μs (which is on the order of free induction decay time).

We fitted the decay curves to Gaussian functions

$$G(t,\tau) = A(\tau)([1 - C(\tau)]\mathrm{e}^{-M(\tau)t^2/2} + C(\tau)), \tag{5}$$

where A (amplitude), M (second moment) and C (asymptote) are used as fitting parameters that vary with the DQ time τ. As shown by the decay curves in figure 2 and by the behavior of the fitting parameters in figures 3 and 4, the system exhibits an interesting dynamics as a function of the DQ-time evolution. This is in contrast to what was observed in 3D systems [12, 13], where the decay simply becomes monotonically faster as the DQ-time τ is increased. The difference can be traced to the fact that the constrained coupling topology in 1D systems allow for a slower decay dominated by NN interactions, while in 3D systems the decay is more rapid and diffusion-like. We can compare for example the decay of calcium fluoride (CaF_2) [13] with FAp. While the minimum distance between NNs is quite similar ($r_{CaF_2} = 0.27$ nm versus $r_{FAp} = 0.34$ nm) the decay time is much faster for CaF_2, both for short and especially for longer DQ-times, where it can be almost an order of magnitude faster. In the following, we present a theoretical model of the observed behavior in 1D systems.

3. Theoretical model and interpretation

To gain insight into the decay behavior, we model both the dipolar Hamiltonian and the DQ Hamiltonian as 1D, NN interactions, neglecting the smaller contributions from long-range couplings in the chain and between chains. This approximation is justified in the short time limit that we explore experimentally [21].

3.1. Decay amplitude

The NN DQ Hamiltonian is known to be analytically solvable in 1D by means of a Jordan–Wigner mapping [30] onto a system of free fermions. The density operator describing the thermal initial state evolving under the DQ Hamiltonian can be expressed in terms of canonical fermionic operators as [31, 32]

$$\begin{aligned}\rho_{\mathrm{th}}(\tau) = &\sum_{p-q\,\in\,\mathrm{even}} \mathrm{i}^{-(p+q)} f_{pq}(2\tau)(c_p^\dagger c_q + c_q^\dagger c_p - \delta_{p,q}) \\ &+ \mathrm{i} \sum_{p-q\,\in\,\mathrm{odd}} \mathrm{i}^{-(p+q)} f_{pq}(2\tau)(c_p^\dagger c_q^\dagger - c_q c_p),\end{aligned} \tag{6}$$

where the first term describes ZQ coherences, $\rho^{(0)}(\tau)$, and the second term DQ coherences, $\rho^{(2)}(\tau)$. Here we defined the fermionic operators $c_p = (\prod_{k<p} \sigma_z^k)\sigma_-^p$ and

$$f_{pq}(\tau) = \frac{2}{n+1} \sum_k (-1)^p \sin(p\kappa) \sin(q\kappa) \mathrm{e}^{-2\mathrm{i}bt\cos\kappa}, \tag{7}$$

where N is the chain length and $\kappa = \frac{\pi k}{N+1}$.

We are interested in following the decay of these states under the dipolar Hamiltonian. We thus consider the normalized signal as a function of decay time t:

$$S(t,\tau) = \mathrm{Tr}\{\delta\rho_{\mathrm{o}}(\tau) U_{\mathrm{dip}}(t) \delta\rho(\tau) U_{\mathrm{dip}}^\dagger(t)\} / \mathrm{Tr}\{\delta\rho_{\mathrm{o}}(\tau)\delta\rho(\tau)\}. \tag{8}$$

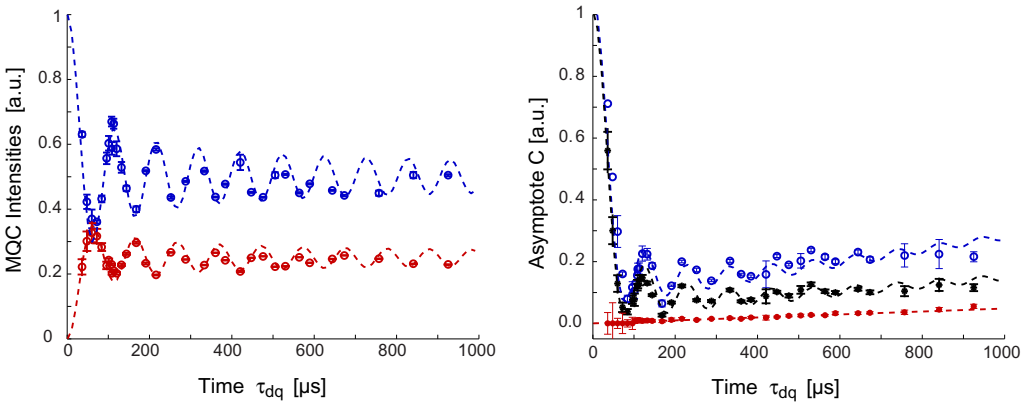

Figure 3. Left: evolution of multiple quantum coherence intensities (A_{ZQ} blue, A_{DQ} red) starting from the thermal equilibrium initial state. The MQC intensities are obtained from the amplitude parameter $A(\tau)$ when fitting the decay curves (error bars are also obtained from the fitting). The MQC intensities are then fitted by functions (blue and red dashed lines) obtained from the analytical model of the DQ Hamiltonian with NN couplings (equations (A.6) and (A.7)), yielding a dipolar coupling $7.7 \times 10^3\,\mathrm{rad\,s^{-1}}$. Right: asymptotes of the experimental decay curves (C_{ZQ} blue, C_{DQ} red, C_{total} black). The curves were fitted by equation (9) with an additional linear term in τ, giving a dipolar coupling of $7.676 \times 10^3\,\mathrm{rad\,s^{-1}}$.

We first note that the amplitude $A(\tau)$ in equation (5) is given either by the total signal, $A_{\mathrm{S}}(\tau) = \mathrm{Tr}\{\delta\rho_{\mathrm{o}}(\tau)\delta\rho(\tau)\}$ or by the MQC intensities, $A_{m\mathrm{Q}}(\tau) = \mathrm{Tr}\{\delta\rho_o^{(m)}(\tau)\delta\rho^{(m)}(\tau)\}$, at $t = 0$. This is shown in figure 3(a), where we plot $A_{\mathrm{ZQ}}(\tau)$ and $A_{\mathrm{DQ}}(\tau)$. Since the total signal decays during the DQ evolution time τ (due to imperfection in the creation of the NN DQ Hamiltonian because of pulse errors, higher-order corrections in the Magnus expansion as well as errors due to long-range couplings [21]) we normalize these amplitudes by the total signal amplitude $A_{\mathrm{S}}(\tau)$. Upon this correction it is possible to fit the amplitudes to well-known analytical solutions for the zero- ($I^{(0)}$) and DQ ($I^{(2)}$) intensities [29] (see also the appendix). From these fits, considering an infinite chain, (figure 3) we find a NN dipolar constant $b = 7.7 \times 10^3\,\mathrm{rad\,s^{-1}}$. The value of the dipolar constant b agrees very well with the one obtained from similar measurements done on a different FAp crystal [9, 21] and also with the theoretical value $b = 8.17 \times 10^3\,\mathrm{rad\,s^{-1}}$ obtained from the known structure of FAp.

3.2. Long-time asymptote

The only terms that contribute to the asymptote C are those that commute with the dipolar Hamiltonian, i.e. $C = \mathrm{Tr}\{\rho_{\mathrm{i}}^c(\tau)\rho_{\mathrm{o}}^c(\tau)\}/\mathrm{Tr}\{\rho(\tau)\rho_{\mathrm{o}}(\tau)\}$, such that $[\mathcal{H}_{\mathrm{dip}}, \rho^c] = 0$. In the NN approximation, ρ^c contains only the population terms (i.e. $p = q$ in equation (6)); hence we obtain

$$C(\tau) = \left(\frac{1}{N}\sum_p (-1)^p f_{pp}(2\tau)\right)^2 = \left(\frac{1}{N}\sum_k \cos(4\tau\cos\kappa)\right)^2. \tag{9}$$

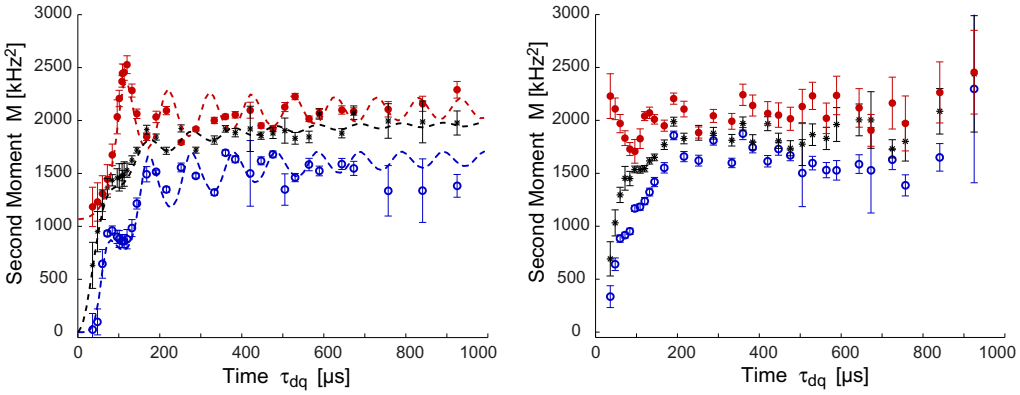

Figure 4. Decay rates of the different MQ components as a function of DQ evolution time τ for (left) the thermal and (right) end-polarized initial state. Points are experimental results obtained from the fitting of individual decay curves (such as in figure 2) for each DQ-time τ. Error bars are estimated from fitting the decay curves with the function in equation (5)). The dashed lines are $\mu\, M(b, \tau)$, where $M(b, \tau)$ are the analytical curves in the appendix for $N = 100$ with $b = 7.9 \times 10^3$ rad s^{-1}. The total signal moment (black stars) was scaled by a factor $\mu = 1.7$, the ZQ moment (blue circles) by a factor 1.8 and the DQ moment (red, dots) by 1.5.

As ρ^c only contains ZQ terms, we expect a zero asymptote for the DQ intensities. We use the function $C(\tau)$ with an additional linear term in τ to fit the experimentally obtained asymptotes. This is shown in figure 3(b). The dipolar coupling (b) is used as a fitting parameter and the value obtained from the fit, $b = 7.676 \times 10^3$ rad s^{-1}, agrees very well with the MQC fittings. The linear increase of the asymptote with time is due to errors in the implementations of the DQ evolution, as terms which are not ZQ and DQ coherences appear as an increased population term when normalizing the signal.

3.3. Decay rate

To determine the decay rate, we analyze the evolution by a short time expansion [33], $\rho_{\mathrm{i}}(t, \tau) \approx \rho_{\mathrm{i}}(\tau) - it[\mathcal{H}_{\mathrm{dip}}, \rho_{\mathrm{i}}(\tau)] - \frac{t^2}{2}[\mathcal{H}_{\mathrm{dip}}, [\mathcal{H}_{\mathrm{dip}}, \rho_{\mathrm{i}}(\tau)]]$, with a corresponding signal, $S(t, \tau) \propto \mathrm{Tr}\{\rho_{\mathrm{i}}(t, \tau)\rho_{\mathrm{o}}(\tau)\}$. We note that the first order term does not give any contribution to the signal [34], so we calculate the second moment

$$M = \frac{\mathrm{Tr}\{[\mathcal{H}_{\mathrm{dip}}, [\mathcal{H}_{\mathrm{dip}}, \rho_{\mathrm{i}}(\tau)]]\rho_{\mathrm{o}}(\tau)\}}{\mathrm{Tr}\{\rho_{\mathrm{i}}(\tau)\rho_{\mathrm{o}}(\tau)\}} = \frac{\mathrm{Tr}\{[\mathcal{H}_{\mathrm{dip}}, \rho_{\mathrm{i}}(\tau)][\rho_{\mathrm{o}}(\tau), \mathcal{H}_{\mathrm{dip}}]\}}{N2^N}. \tag{10}$$

We can further calculate the contributions to the second moment arising from the zero- and DQ terms of the density operator

$$M^{(m)} = \frac{\mathrm{Tr}\{[\mathcal{H}_{\mathrm{dip}}, \rho^{(m)}(\tau)][\rho^{(m)}(\tau), \mathcal{H}_{\mathrm{dip}}]\}}{\mathrm{Tr}\{\rho^{(m)}(\tau)\rho^{(-m)}(\tau)\}}. \tag{11}$$

These functions can be calculated analytically (see the appendix), thanks to the mapping to fermionic operators. We used these functions to analyze the second moments in figure 4, fitting

the experimental momentum $M_{\rm exp}$ to the analytical functions $\mu M(b)$. From the fits we obtained $b = 7.9 \times 10^3\,{\rm rad\,s^{-1}}$ and $\mu \approx 1.7$. This indicates that while the variations of M with the DQ evolution time τ are well in agreement with the analytical model and the expected dipolar coupling strength, the experimental second moment $M_{\rm exp}$ is larger than expected from this model. This suggests that other mechanisms contribute to the decay, including longer range couplings and control errors in the state preparation.

Some features of the second moments are worth pointing out. For small τ times, the decay rate of the ZQ intensities (and of the signal) goes to zero, as indeed the initial state is an equilibrium state that commutes with the dipolar Hamiltonian. Instead, $M^{(2)}$ has a finite asymptote, $b^2/12$, for $\tau \to 0$ (see equations (A.10) and (A.13)): mathematically, this is because both the commutator and the DQ intensities go to zero with τ; physically, this means that as soon as some DQ term is created in the state, it will decay with a finite rate under the dipolar Hamiltonian.

The second moments of both MQC intensities then oscillate in time with τ, with the DQ moment always being larger than the ZQ one, $M^{(2)} > M^{(0)}$. This can be understood by their different behavior under the dipolar Hamiltonian. Consider the ZQ state, $\rho^{(0)}_{\rm th}(\tau)$ (first line in equation (6)) and the 'flip-flop' term of the dipolar Hamiltonian, $\mathcal{H}_{xx} = b\sum_j (c_j^\dagger c_{j+1} + c_{j+1}^\dagger c_j)$. If we had considered periodic boundary conditions (instead of an open chain), these two operators would have commuted. Thus we expect their contribution to the second moment to be small and decreasing with the chain length N. In contrast, the contribution of $\mathcal{H}_{xx}$ to the second moment of $\rho^{(2)}(\tau)$ is on the same order as the contribution from $\mathcal{H}_{zz} = b\sum_j \sigma_z^j \sigma_z^{j+1}$, thus yielding an overall faster decay rate. We can understand this behavior more intuitively. Here we defined quantum coherence with respect to the total magnetization along the z-axis [35], Σ_z, which also sets the quantization axis of the system. Indeed, we only retained the part of the dipolar interaction that commutes with Σ_z. Thus we expect terms in the system state that commute with Σ_z (such as ZQ terms) to decay more slowly than terms that do not.

It is interesting to note that both the ZQ and DQ second moments are higher when the corresponding MQC intensity is smaller (see also figure A.1 in the appendix). By analyzing the state in equation (6), we can see that times τ of local maxima for $I^{(0)}(\tau)$ correspond to maxima for the function $f_{pp}(2\tau)$, which indicates that the state is localized around single-spin polarization states, σ_z^j, while at other times the ZQ intensities have stronger contributions from many-spin correlations (three and higher). Correspondingly, local maxima for $I^{(2)}(\tau)$ correspond to higher contributions from localized two-spin DQ states in $\rho(\tau)$, $\sigma_+^j \sigma_-^{j+1}$. We thus found that the decay rates depends not only on the coherence order of the state, but also on whether the state is localized or contains a larger number of spin correlations. While these two effects could not be distinguished clearly in 3D experiments, as it was not possible to determine the precise states created, the 1D case provides further insights into the decay dynamics. We can further explore these differences by studying the decay of other correlated states.

4. Comparison of initial states

In order to study the dependence of the decay rate on the coherence order and the number of correlated spins, we evolved different initial states under the DQ Hamiltonian. Besides the thermal state, we considered two other initial states: the 'end-polarized' state $\delta\rho_{\rm end} \propto (\sigma_z^1 + \sigma_z^N)$ [8, 9] and a state rotated in the transverse plane, $\Sigma_x = \sum_j \sigma_x^j$. We prepared the first

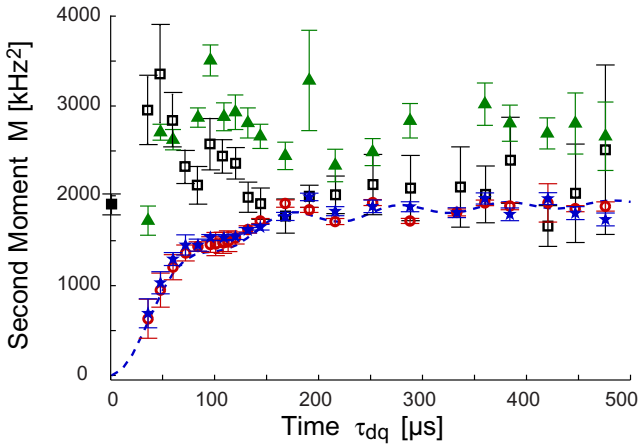

Figure 5. Decay rates of the total signal as a function of evolution time τ for different initial states: thermal state $\delta\rho_{\text{th}}$ (blue stars), end-polarized state $\delta\rho_{\text{end}}$ (red circles); transverse polarization, $\delta\rho_x$ (black squares) and the state presenting a broader distribution of MQC, $\delta\rho_{xx}$ (green triangles). The black filled square at $\tau = 0$ is the second moment of the free-induction decay. As the $\delta\rho_x(\tau)$ states present oscillations in the decay (similar to the free-induction decay, see figure 2) we fitted their decay to the function [28] $A[(1-C)\text{sinc}(m_2 t)\,\text{e}^{-m_1 t^2/2} + C]$, with the second moment given by $M = m_1 + m_2^2/3$. The dashed line is the analytical model for the thermal state second moment, as in figure 4.

state by the two-pulse scheme introduced in [8], while the second state can be prepared by a simple collective rotation of the spins.

The end-polarized state exhibits a transport-like dynamics under the DQ Hamiltonian [11]; although the transport is dispersive [31, 36], we expect the state to remain fairly localized at short times and thus to show similar decay behavior as the thermal state. In contrast, the initial state $\delta\rho_x \sim \Sigma_x$ quickly evolves into many-spin correlations. Indeed, if we consider for example evolution of the first spin in the chain $\delta\rho_{x_1} \sim \sigma_x^1$, we obtain

$$\delta\rho_{x_1}(\tau) = \sum_{p\in\text{odd}} \text{Im}[\text{i}^{-p} f_{1p}(\tau)](c_p^\dagger + c_p) - \text{i} \sum_{p\in\text{even}} \text{Im}[\text{i}^{-p} f_{1p}(\tau)](c_p^\dagger - c_p). \tag{12}$$

Here we note that the fermionic operators c_p represent highly delocalized states, since we have, e.g., $c_p^\dagger + c_p = \sigma_z^1 \ldots \sigma_z^{p-1}\sigma_x^p$. Similar expressions can be found for the evolution of the other spins in the chain and thus for $\delta\rho_x(\tau)$. While this state presents large spin correlations, its coherence number is still quite low, with mostly one- and three-quantum coherences [31]. In order to investigate the decay of larger coherence orders, we rotate the state $\delta\rho_x(\tau)$ with a $\pi/2$-pulse around the y-axis before letting it evolve freely. The resulting state, $\delta\rho_{xx}$, contains all even quantum coherence orders with a binomial distribution and it is thus more similar to the states that can be obtained in 3D systems [27].

We compare the decay rates (second moment) of these four different states in figure 5. When the evolution under the DQ-Hamiltonian is short, the decay rate of $\delta\rho_{\text{th}}$ and $\delta\rho_{\text{end}}$ is small, as expected. Although $\delta\rho_{xx}$ has a small decay rate at short times, since it has main contributions from ZQ coherences, the second moment increases quickly with τ. In comparison, $\delta\rho_x$ has a fast decay even when it has not evolved under the DQ-Hamiltonian (indeed for $\tau = 0$ we

recover the second moment of the free-induction decay). At larger τ the second moment still remains slightly larger than the second moments of $\delta\rho_{\rm th}$ and $\delta\rho_{\rm end}$. Indeed at larger τ all the states becomes fairly delocalized because of the dispersive character of the equal-coupling DQ Hamiltonian [36]. Thus these different states highlight different behaviors of multi-spin correlated states, which depend on the number of spins in the correlated state (with faster decay for larger spin correlation number) and separately on the coherence number.

5. Conclusions

In this paper we investigated the dependence of decoherence rate on the state characteristics of a many-spin system. Since the decay process is non-Markovian, but it is due to a highly correlated spin bath, we found a very rich dynamics, where decoherence rates (quantified by the second moment of the decay) depend in a non-trivial way on the degree of localization of the state as well as on its coherence with respect to the quantization basis. In particular we found that large spin clusters, with correlations established among many spins, decay faster under a correlated bath, even if their coherence order is not very large. This is in contrast to the decay under simple dephasing, where the coherence order (and for pure states, the entanglement) is critical in determining the decay rate [37]. While it was not possible to separate the coherence order and the number of correlated spins in the dynamics of 3D spin systems (as they grow at the same time), here we were able to get a deeper insight by using spin chains and exploring different initial states. In addition we found that restricting the dynamics in one dimension slows down the decay, which could be beneficial to create larger coherent quantum states.

Acknowledgments

This work was partially funded by NSF under grant DMG-1005926 and by AFOSR YIP.

Appendix. Calculation of the second moment

Here we provide explicit expressions for the second moment of the decay under the dipolar Hamiltonian of the thermal state evolved under the DQ Hamiltonian for a time τ. Using the second moment to estimate the decay rate is justified by a short time expansion of the signal

$$S(t,\tau)\approx S(\tau)\left(1-M\frac{t^2}{2}\right)=\mathrm{Tr}\{\delta\rho(\tau)^2\}\left(1-\frac{\mathrm{Tr}\{[\mathcal{H}_{\rm dip},\rho(\tau)][\rho(\tau),\mathcal{H}_{\rm dip}]\}}{\mathrm{Tr}\delta\rho(\tau)^2}\frac{t^2}{2}\right). \tag{A.1}$$

We can calculate the contributions to the second moment arising from the ZQ and DQ terms of the density operator

$$M^{(m)}=\frac{\mathrm{Tr}\{[\mathcal{H}_{\rm dip},\rho^{(m)}(\tau)][\rho^{(m)}(\tau),\mathcal{H}_{\rm dip}]\}}{\mathrm{Tr}\{\rho^{(m)}(\tau)\rho^{(-m)}(\tau)\}}. \tag{A.2}$$

Further, writing the dipolar Hamiltonian as

$$\mathcal{H}_{\rm dip}=2\mathcal{H}_{zz}-\mathcal{H}_{xx},\quad \mathcal{H}_{zz}=\sum_{ij}b_{ij}\sigma_z^i\sigma_z^j,\quad \mathcal{H}_{xx}=\sum_{ij}b_{ij}(\sigma_x^i\sigma_x^j+\sigma_y^i\sigma_y^j), \tag{A.3}$$

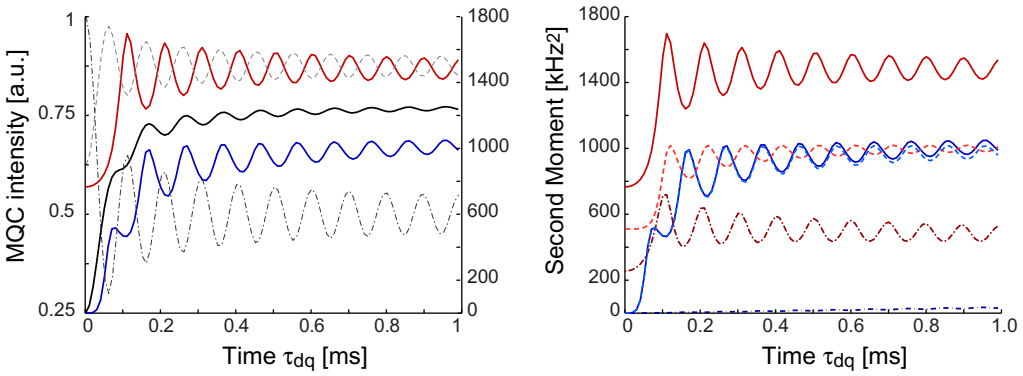

Figure A.1. Analytical solutions to second moments for $N = 400$ spins. Left: second moment for the ZQ intensities (blue), DQ (red) and total signal (black). In lighter gray: MQC intensities ($I^{(0)}$, ZQ, dash-dotted line, $I^{(2)}$, DQ, dashed line) highlighting the anti-correlation with the momentum oscillations. For an easier visualization, we plot $I^{(2)} + 0.625$. Right: contributions of the $\mathcal{H}_{xx}$ (dash-dotted) and $\mathcal{H}_{zz}$ (dashed) Hamiltonians to the total (solid) second momenta for ZQ (blue lines) and DQ (red lines) intensities. We note that the second moment from $\mathcal{H}_{xx}$ is almost zero for the ZQ intensities, the small increase at larger DQ times τ_{dq} is due to finite-length chain effects.

we can also separate the contributions from the $\mathcal{H}_{zz}$ and $\mathcal{H}_{xx}$ parts of the dipolar Hamiltonian, as they simply add up (there are no contributions from cross-terms). We can thus define each contribution as

$$M_{aa}^{(n)} = \mathrm{Tr}\left\{[\mathcal{H}_{aa}, \rho^{(n)}(\tau)][\mathcal{H}_{aa}, \rho^{(n)}(\tau)]\right\}/(N2^N) \tag{A.4}$$

yielding the total second moment

$$M = M_{zz} + 2M_{xx} = I^{(0)}(M_{zz}^{(0)} + 2M_{xx}^{(0)}) + I^{(2)}(2M_{zz}^{(2)} + 4M_{xx}^{(2)})/(N2^N), \tag{A.5}$$

where $I^{(m)}$ are the MQC intensities [29] (see figure A.1)

$$I^{(0)}(\tau) = \frac{1}{N}\sum_k \cos(4\tau\cos\kappa)^2, \tag{A.6}$$

$$I^{(2)}(\tau) = \frac{1}{2N}\sum_k \sin(4\tau\cos\kappa)^2. \tag{A.7}$$

Using the state in equation (6) we find the contribution from $\mathcal{H}_{zz}$:

$$M_{zz} = \frac{16}{N}\left[\sum_{p\neq q}|f_{p,q}(2\tau)|^2 - \sum_{q=2}^{N}\left(|f_{q,q-1}(2\tau)|^2 + |f_{q,q-2}(2\tau)|^2 + |f_{1,q}(2\tau)|^2\right)\right] \tag{A.8}$$

which is given by the sum of the ZQ and DQ contributions (see figure A.1):

$$M_{zz}^{(0)}I^{(0)} = \frac{16}{N}\left[\sum_{\substack{p\neq q,\\ p-q\in\text{even}}}|f_{p,q}(2\tau)|^2 - \sum_{q=2}^{N}|f_{q,q-2}(2\tau)|^2 - \sum_{\substack{p\neq 1,\\ p\in\text{odd}}}|f_{1,q}(2\tau)|^2\right], \tag{A.9}$$

$$M_{zz}^{(2)} I^{(2)} = \frac{8}{N}\left[\sum_{p-q\in\text{odd}} |f_{p,q}(2\tau)|^2 - \sum_{q=1}^{N} |f_{q,q-1}(2\tau)|^2 - \sum_{p\in\text{even}} |f_{1,p}(2\tau)|^2\right]. \tag{A.10}$$

From the commutator with $\mathcal{H}_{xx}$ we obtain

$$M_{xx} = \frac{4(N-1)}{N} - \frac{2}{N}\sum_{p,q}\left[f_{p+1,q}(2\tau) - f_{p-1,q}(2\tau)\right]\left[f_{p,q+1}(2\tau) - f_{p,q-1}(2\tau)\right] \tag{A.11}$$

which can be further decomposed into the ZQ and DQ components:

$$M_{xx}^{(0)} I^{(0)} = M_{xx}(\tau) - I^{(2)}(\tau) M_{xx}^{(2)}(\tau), \tag{A.12}$$

$$M_{xx}^{(2)} I^{(2)} = \frac{2}{N}\sum_{p-q\in\text{odd}} |f_{p,q}(2\tau) - f_{q-1,p+1}(2\tau)|^2. \tag{A.13}$$

References

[1] Zurek W H 1991 Decoherence and the transition from quantum to classical *Phys. Today* **44**(10) 36

[2] Fischer J and Loss D 2009 Dealing with decoherence *Science* **324** 1277–8

[3] Viola L, Knill E and Lloyd S 1999 Dynamical decoupling of open quantum systems *Phys. Rev. Lett.* **82** 2417–21

[4] Biercuk M J, Uys H, VanDevender A P, Shiga N, Itano W M and Bollinger J J 2009 Optimized dynamical decoupling in a model quantum memory *Nature* **458** 996–1000

[5] Ryan C A, Hodges J S and Cory D G 2010 Robust decoupling techniques to extend quantum coherence in diamond *Phys. Rev. Lett.* **105** 200402

[6] Álvarez G A, Ajoy A, Peng X and Suter D 2010 Performance comparison of dynamical decoupling sequences for a qubit in a rapidly fluctuating spin bath *Phys. Rev.* A **82** 042306

[7] Shukla A and Mahesh T S 2011 arXiv:1110.1473

[8] Cappellaro P, Ramanathan C and Cory D G 2007 Dynamics and control of a quasi-one-dimensional spin system *Phys. Rev.* A **76** 032317

[9] Kaur G and Cappellaro P 2012 Initialization and readout of spin chains for quantum information transport *New J. Phys.* **14** 083005

[10] Teshima K, Lee S, Ishizaki T, Mori S, Mori C, Yubuta K, Ichiki T, Shishido T and Oishi S 2011 Novel fast and easy growth of highly crystalline, idiomorphic fluorapatite crystals via an atmospheric pressure plasma-assisted flux coating method *Cryst. Eng. Commun.* **13** 1749–51

[11] Cappellaro P, Ramanathan C and Cory D G 2007 Simulations of information transport in spin chains *Phys. Rev. Lett.* **99** 250506

[12] Krojanski H G and Suter D 2004 Scaling of decoherence in wide NMR quantum registers *Phys. Rev. Lett.* **93** 090501

[13] Cho H J, Cappellaro P, Cory D G and Ramanathan C 2006 Decay of highly correlated spin states in a dipolar-coupled solid: NMR study of CaF_2 *Phys. Rev.* B **74** 224434

[14] Lovrić M, Krojanski H G and Suter D 2007 Decoherence in large quantum registers under variable interaction with the environment *Phys. Rev.* A **75** 042305

[15] Sanchez C M, Pastawski H M and Levstein P R 2007 Time evolution of multiple quantum coherences in NMR *Physica* B **398** 472–5

[16] Álvarez G A, Danieli E P, Levstein P R and Pastawski H M 2010 Decoherence as attenuation of mesoscopic echoes in a spin-chain channel *Phys. Rev.* A **82** 012310

[17] Álvarez G A and Suter D 2010 NMR quantum simulation of localization effects induced by decoherence *Phys. Rev. Lett.* **104** 230403

[18] Cetina M, Bylinskii A, Karpa L, Gangloff D, Beck K M, Ge Y, Scholz M, Grier A T, Chuang I and Vuletic V 2013 One-dimensional array of ion chains coupled to an optical cavity *New J. Phys.* **15** 053001
[19] Ajoy A and Cappellaro P 2013 Quantum simulation via filtered Hamiltonian engineering: application to perfect quantum transport in spin networks *Phys. Rev. Lett.* **110** 220503
[20] Cho G and Yesinowski J P 1993 Multiple-quantum NMR dynamics in the quasi-one-dimensional distribution of protons in hydroxyapatite *Chem. Phys. Lett.* **205** 1–5
[21] Zhang W, Cappellaro P, Antler N, Pepper B, Cory D G, Dobrovitski V V, Ramanathan C and Viola L 2009 NMR multiple quantum coherences in quasi-one-dimensional spin systems: comparison with ideal spin-chain dynamics *Phys. Rev.* A **80** 052323
[22] Cappellaro P, Hodges J S, Havel T F and Cory D G 2007 Control of qubits encoded in decoherence-free subspaces *Laser Phys.* **17** 545–51
[23] Rufeil-Fiori E, Sánchez C M, Oliva F Y, Pastawski H M and Levstein P R 2009 Effective one-body dynamics in multiple-quantum NMR experiments *Phys. Rev.* A **79** 032324
[24] Yen Y-S and Pines A 1983 Multiple-quantum NMR in solids *J. Chem. Phys.* **78** 3579–82
[25] Ramanathan C, Cho H, Cappellaro P, Boutis G S and Cory D G 2003 Encoding multiple quantum coherences in non-commuting bases *Chem. Phys. Lett.* **369** 311
[26] Haeberlen U 1976 *High Resolution NMR in Solids: Selective Averaging* (New York: Academic)
[27] Baum J, Munowitz M, Garroway A N and Pines A 1985 Multiple-quantum dynamics in solid state NMR *J. Chem. Phys.* **83** 2015–25
[28] Abragam A and Goldman M 1982 *Nuclear Magnetism: Order and Disorder* (Oxford: Clarendon)
[29] Fel'dman E B and Lacelle S 1996 Multiple quantum NMR spin dynamics in one-dimensional quantum spin chains *Chem. Phys. Lett.* **253** 27–31
[30] Jordan P and Wigner E 1928 About the pauli exclusion principle *Z. Phys.* B **47** 631
[31] Ramanathan C, Cappellaro P, Viola L and Cory D G 2011 Experimental characterization of coherent magnetization transport in a one-dimensional spin system *New J. Phys.* **13** 103015
[32] Doronin S, Maksimov I and Fel'dman E 2000 Multiple-quantum dynamics of one-dimensional nuclear spin systems in solids *J. Exp. Theor. Phys.* **91** 597–609
[33] Doronin S I, Fel'dman E B and Maximov I I 2004 Line shapes of multiple quantum NMR coherences in one-dimensional quantum spin chains in solids *J. Magn. Reson.* **171** 37–42
[34] Ajoy A and Cappellaro P 2012 Mixed-state quantum transport in correlated spin networks *Phys. Rev.* A **85** 042305
[35] Cho H J, Ladd T D, Baugh J, Cory D G and Ramanathan C 2005 Multispin dynamics of the solid-state NMR free induction decay *Phys. Rev.* B **72** 054427
[36] Cappellaro P, Viola L and Ramanathan C 2011 Coherent-state transfer via highly mixed quantum spin chains *Phys. Rev.* A **83** 032304
[37] Huelga S F, Macchiavello C, Pellizzari T, Ekert A K, Plenio M B and Cirac J I 1997 Improvement of frequency standards with quantum entanglement *Phys. Rev. Lett.* **79** 3865–8